Polymeric Carbon Nitride (PCN) based heterojunction for Environmental Remediation

Dissertation submitted to

Visvesvaraya National Institute of Technology

in partial fulfilment of the requirements for the award of

the degree

Master of Science

in

Chemistry

by

Palak Kampani (MS23CHM004)

under the guidance of

Prof. Suresh S. Umare

Department of Chemistry

Visvesvaraya National Institute of Technology

Nagpur 440 010 (India)

May 2025

Polymeric Carbon Nitride (PCN) based heterojunction for Environmental Remediation

Dissertation submitted to

Visvesvaraya National Institute of Technology

in partial fulfilment of the requirements for the award of

the degree

Master of Science

in

Chemistry

by

Palak Kampani (MS23CHM004)

under the guidance of

Prof. Suresh S. Umare

Department of Chemistry

Visvesvaraya National Institute of Technology

Nagpur 440 010 (India)

May 2025

©Visvesvaraya National Institute of Technology (VNIT) 2025

Department of Chemistry

Visvesvaraya National Institute of Technology

Declaration

I, Palak Kampani, hereby declare that this dissertation titled "Polymeric Carbon Nitride (PCN) based heterojunction for Environmental Remediation" is carried out by me in the Department of Visvesvaraya National Institute of Technology, Nagpur. The work is original and has not been submitted earlier whole or in part for the award of any degree/diploma at this or any other Institution / University.

Palak Kampani

Date:

Certificate

This to certify that the dissertation titled "Polymeric Carbon Nitride (PCN) based heterojunction for Environmental Remediation" is submitted by Palak Kampani in partial fulfilment of the requirements for the award of the degree of Master of Science in Chemistry, VNIT Nagpur. The work is comprehensive, complete and fit for final evaluation.

Prof. S.S. Umare

Professor, Dept, VNIT, Nagpur

Head, Department of Chemistry

VNIT, Nagpur

Date:

VISVESVARAYA NATIONAL INSTITUTE OF TECHNOLOGY, NAGPUR

Non-Plagiarism Certificate

Certified that M.Sc. Dissertation titled "Polymeric Carbon Nitride (PCN) based heterojunction for Environmental Remediation" submitted by Palak Kampani Enrollment No. MS23CHM004 ID No. 30164 has been checked for plagiarism using TURNITIN software and the overlap is found within the prescribed limits. A summary of the report is given below:

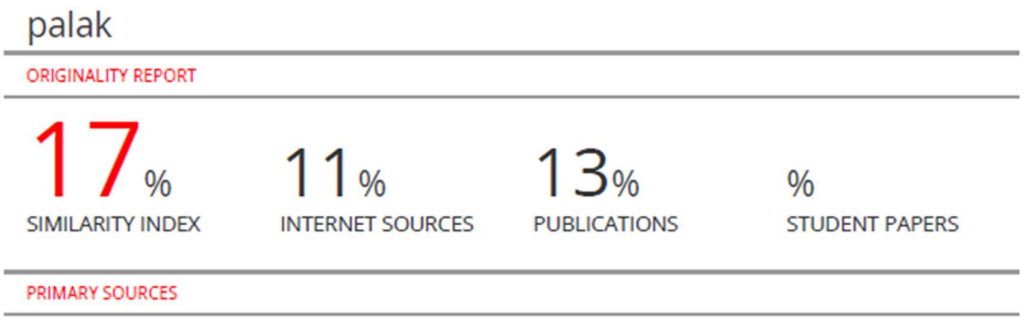

Palak Kampani
MS23CHM004
Id No: 30164

Prof. S.S. Umare
Department of Chemistry
VNIT, Nagpur

Acknowledgement

I would like to express my profound gratitude to my project supervisor, Prof. Suresh S. Umare, Department of Chemistry, for his encouragement and patience during the course of my M.Sc. project. I am very grateful for his guidance and disciplinary inspiration which has helped me to improve my personal skills. I extend my thanks to the Department of Chemistry, for providing the necessary facilities to undertake the project efficiently.

I convey my sincere gratitude to **Mr. Swapnil Sarkar**, Doctoral Fellow at VNIT, Nagpur for his constant support and guidance. I am also thankful to **Mr. Pritam Ramteke, Ms. Ruchika, Mrs. Renuka and Ms. Anjali**, Doctoral fellow at VNIT, Nagpur for their tremendous mentorship in the lab and my friend Mr. Tanmay for his help in the lab.

Finally, I would like to thank my family and friends whose constant support and blessings helped me throughout the project.

Palak Kampani

(MS23CHM004)

Abstract

Polymeric Carbon Nitride (PCN) based heterojunction for Environmental Remediation

Palak Kampani (MS23CHM004) and Suresh S. Umare

Materials and Catalysis Laboratory, Department of Chemistry, Visvesvaraya National Institute of Technology (VNIT), Nagpur, India

With rapid industrialization, the environmental pollution generated by contaminated wastes from various industries is emerging as a global calamity. Visible light-assisted semiconductor photocatalysis has been extensively used for environmental remediation due to its various benefits such as no generation of toxic waste, energy efficient and green process.

Polymeric carbon nitride (PCN) is a metal free semiconductor exhibiting versatile photocatalytic activity and widely used in environmental remediation. However, low specific surface area, high charge carrier recombination rate, limited surface adsorption are some of the drawbacks of PCN. The incorporation of borophene doped poly (triazine) imide (PTI) with polymeric carbon nitride leads to the formation of a binary heterostructure demonstrating excellent characteristics like high surface area, efficient charge transfer, optimised photocatalytic performance. In the synthesized binary heterostructure, borophene acts as a mediator thereby allowing for efficient charge transfer between PTI and PCN. The structural and optical properties of the prepared catalysts were analyzed using powder X-ray diffraction (p-XRD), Fourier Transform Infrared Spectroscopy (FTIR), BET surface area analysis, and UV-DRS. The photocatalytic activity of the binary heterostructure were examined for the photodegradation of rhodamine B (RhB) and Cr (VI) reduction. 5(0.5B-PTI)-PCN shows better photocatalytic activity compared to the other (0.5B-PTI)-PCN composite, as well as their individual components. The improved photocatalytic performance of 5(0.5B-PTI)-PCN heterostructure is attributed to the combined effects of reduced electron-hole recombination rate, enhanced surface area, and increased visible light absorption.

List of Figures

Serial No.	Title	Page No.
	Chapter 1	
1.1	Energy transformation diagram for catalysed and non-catalysed reactions	5
1.2	Schematic representation of photocatalytic degradation mechanism on a semiconductor surface	6
1.3	Structure of polymeric g-C_3N_4	9
1.4	Poly (triazine) imide	12
1.5	Structure of borophene cluster	12
	Chapter 2	
2.1	Representation of Bragg's diffraction in crystal structure	19
	Chapter 3	
3.1	p-XRD pattern of various catalysts	26
3.2	FT-IR spectra of PCN, PTI, 0.5B-PTI and 5(0.5B-PTI-PCN)	28
3.3	(a) UV-Visible diffuse reflectance spectra and (b) Kubelka-Munk plot of various catalysts	29
3.4	TEM images of (a) PCN (b) PTI (c) and (d) 5(0.5B-PTI)-PCN	30
3.5	(a) N_2 adsorption-desorption isotherm and (b) pore size distribution of PCN, PTI and 5(0.5B-PTI)-PCN	32
3.6	SEM images of (a) PCN (b) PTI (c) and (d) 5(0.5B-PTI)-PCN (e) EDX Analysis of 5(0.5B-PTI)-PCN	34

3.7.1	(a) Photocatalytic RhB (20 mg/L) degradation of RhB and (b) percentage degradation of RhB (20mg/L) at 30 minutes using various catalysts	35
3.7.2	(a) Photocatalytic Cr (VI) performance and (b) percentage reduction of Cr (VI) to Cr (III) at 30 min using various catalysts	37
3.8	(a) Effect of quenchers on photocatalytic degradation of RhB (20 mg/L) and (b) Corresponding percentage degradation in presence of quenchers	38
3.9	(a) Effect of pH on degradation of RhB (20mg/L) (b) corresponding percentage degradation of RhB (20mg/L) at different pH	40
3.10	Recyclability studies of RhB degradation using 5(0.5B-PTI)-PCN heterostructure up to five cycles	41

Nomenclature

Abbreviation	Full Form
ROS	Reactive Oxygen Species
AOP	Advanced Oxidation Process
VB	Valence Band
CB	Conduction Band
h^+	Hole
e^-	Electron
RhB	Rhodamine B dye
PCN	Polymeric Carbon Nitride
PTI	Poly (triazine) imide
B-PTI-PCN	Borophene – Poly (triazine) imide-Polymeric Carbon Nitride Composite
XRD	X-Ray diffraction
FT-IR	Fourier Transform Infrared Spectroscopy
UV-DRS	UV-Visible Diffuse Reflectance Spectroscopy
BET	Brunauer–Emmett–Teller
HR-TEM	High Resolution Transmission Electron Microscopy
SEM	Scanning Electron Microscopy

Contents

Serial No.	Title	Page No.
	Chapter 1	
	Introduction	
1.1	**Introduction**	1
1.2	**Pollution due to pharmaceuticals**	1
1.3	**Pollution due to heavy metals**	1
1.3.1	Heavy metal selected for study: Chromium	2
1.4	**Various Methods for Removal of Pollutants**	2
1.4.1	Adsorption	2
1.4.2	Membrane Treatment – Reverse Osmosis	3
1.4.3	Biological Methods	3
1.4.4	Chemical Oxidation/Reduction	3
1.4.5	Chlorination	3
1.4.6	Chemical Precipitation	4
1.5	**Catalysis**	4
1.5.1	Homogeneous catalysis	5
1.5.2	Heterogeneous catalysis	5
1.6	**Photocatalysis**	5
1.6.1	Mechanism	6
1.6.2	Various semiconducting materials used for photocatalysis	7
	a. Metal oxides	7
	b. Metal sulphides and selenides	8
	c. Carbon-based materials	8
1.7	**Graphitic Carbon Nitride: A metal free photocatalyst**	8
1.7.1	Merits of g-C_3N_4	9
1.7.2	Demerits of g-C_3N_4	10
1.7.3	**Strategies to overcome the limitations of g-C_3N_4**	10
1.7.3.1	Doping	10
1.7.3.2	Nanostructure Designing	11

1.7.3.3	Heterostructure Designing/Composite	11
1.7.3.4	Sensitization	11
1.8	**Poly (triazine) imide**	11
1.9	**Borophene**	12
1.10	**Aims and Objective**	13
1.11	**Overview of Thesis**	14
1.12	**References**	15
	Chapter 2	
	Synthesis and Characterization Methods	
2.1	**Chemicals**	17
2.2	**Methods of Preparation**	17
2.2.1	Preparation of PCN	17
2.2.2	Preparation of borophene/Exfoliation of Boron	17
2.2.3	Preparation of PTI	17
2.2.4	Preparation of B-PTI	18
2.2.5	Preparation of (B-PTI)-PCN Heterostructure	18
2.3	**Characterization Techniques**	18
2.3.1	Powder X-ray Characterization	19
2.3.2	UV-Visible Spectroscopy	20
2.3.3	UV-Vis Diffuse Reflectance Spectroscopy (UV-DRS)	20
2.3.4	Fourier Transform Infrared Spectroscopy (FT-IR)	21
2.3.5	Surface area and pore size distribution	22
2.3.6	High-Resolution Transmission Electron Microscopy (HR-TEM)	22
2.3.7	Evaluation of Photocatalytic Activity	23
2.4	**References**	25
	Chapter 3	
	Results and Discussion	
3.1	**Crystal Structure, Phase, and Structural Analysis**	26
3.2	**FT-IR (Fourier Transform Infrared Spectroscopy)**	28

3.3	**Optical Property and Charge Separation Efficiency**	29
3.4	**HR-TEM (High-Resolution Transmission Electron**	31
3.5	**Microscopy)**	
3.6	**Surface area and pore size distribution**	32
3.7.1	**SEM (Scanning Electron Microscope)**	34
3.7.2	**RhB degradation**	35
3.8	**Cr (VI) reduction**	37
3.9	**Effect of Quenchers on RhB degradation**	38
3.10	**Photocatalytic degradation of RhB at different pH**	40
3.11	**Recyclability Studies of 5(0.5B-PTI)-PCN**	41
	References	42
	Chapter 4	
	Summary and Conclusions	
4.1	**Summary and future aspects**	43

CHAPTER 1

INTRODUCTION

This chapter provides the brief overview to various pollutants present in the water bodies, several methods for their removal, utilization of g-C_3N_4 based photocatalyst for environmental remediation.

1.1 Introduction

With the advancement of modern industries, the environmental pollution generated by various industries, is emerging as a global crisis. Water constitutes 71% of the planet and is the most essential element on Earth which plays a vital role for the existence of life. Water is becoming more and more contaminated every day from various sources, including human activity. Industrial waste chemicals are among the most prominent of these. The industries use different chemicals to manufacture various products and discard their waste into the water bodies which leads to water pollution. Major sources of water pollutants are: dyeing industries, textile manufacturing, transportation industries, agricultural use of insecticides and pesticides, mining activities and radioactive waste. These waste cause harmful effect on human health, other animals and plants.[1]

1.2 Pollution due to pharmaceuticals

The developments and advancements in medical science have greatly improved human health and led to safer, longer lives which has resulted in a significant demand for pharmaceutical compound synthesis. Due to its excessive use, the existence of these pharmaceutical compounds in both ground and surface water has become serious concern due to its potential toxicity.[2] Pharmaceuticals degrade the water quality and poses serious threat to living organisms.

1.3 Pollution due to heavy metals

Heavy metals can be defined as the group of metals that possess atomic density more than 4 g/cm^3 such as chromium (Cr), cadmium (Cd), mercury (Hg), lead (Pb), arsenic (As), platinum (Pt) group elements.[3] Heavy metal contamination is a severe ecological hazard that endangers all life on planet. The pollutants have a variety of harmful effects on both human health and the environment. The heavy metals reach

the waterways from several different sources either naturally by weathering and breakdown of rocks or man-made activities. The major contributors that have led to increase in the heavy metal pollution include anthropogenic activities, rapid industrialization, urbanization. Heavy metals induces toxicological effects on living organisms. Heavy metal toxicity can lead to various problems such as fatigue, nausea, vomiting, and severe diseases like asthma, skin cancer. The industries that have majorly contributed to heavy metal pollution are metal and paint industries, pulp and paper manufacturing, power plant, steel plant, mining and textile industries.[4]

1.3.1 Heavy metal selected for study: Chromium

Chromium (Cr) is a naturally occurring element present in the Earth's crust, having oxidation states ranging from chromium (II) to chromium (VI).[5] Chromium is a heavy metal that is deposited into the environment as a result of anthropogenic operations such as chromate production, chrome plating, leather tanning stainless steel welding, and nuclear weapon development. Among its six different chemical forms, Chromium (III) and Chromium (VI) are the most relevant to environmental contamination. Chromium in its trivalent state is less hazardous than the hexavalent form and also plays a role in the metabolism of glucose, lipid, and protein. Hexavalent chromium is highly water soluble and extremely dangerous because its solubility allows it to enter the biological membrane of the human body, causing a variety of mutagenic and carcinogenic effects.[6]

1.4 Various Methods for Removal of Pollutants

Several methods have been employed for the treatment of environmental pollution. These methods have been described below:

1.4.1 Adsorption

Adsorption is a wastewater treatment process that removes the contaminants from polluted water. It is a surface phenomenon. The term adsorbent refers to the adsorbing material and adsorbate refers to the material that is adsorbed. Adsorption is classified into two types physisorption and chemisorption depending on the force of interaction present between the adsorbate and the adsorbent. Physisorption is reversible and involves weak Vander Waal forces of interaction. Chemisorption occurs when the

interactions involve strong chemical bonds making the process irreversible. The contaminants (adsorbate) bind to the surface of the adsorbent and are thereby removed from the water bodies.[7]

Limitations: Limited capacity, cost-effective and it create secondary pollution

1.4.2 Membrane Treatment – Reverse Osmosis

Reverse osmosis is a highly efficient method of purifying water with the help of a semi-permeable membrane. Desalination and water treatment procedures make extensive use of reverse osmosis. When pressure is applied, the molecules of the pure solvent pass across a semi-permeable membrane from a low concentration area to a high concentration area, leaving impurities behind. [8]

Limitations: Increased energy consumption, high space requirements and membrane fouling

1.4.3 Biological Methods

It includes the use of biological processes like bioremediation, phytoremediation, to remove the harmful pollutants prevailing in the environment. Bacteria, algae, fungi have the ability to decompose and absorb a wide variety of pollutants.[9]

Limitations: Time consuming method and biological waste management

1.4.4 Chemical Oxidation/Reduction

The pollutants can either be oxidized or reduced thereby getting converted into less harmful substances. [10]

Limitations: Treatment of limited range of pollutants

1.4.5 Chlorination

One of the popular techniques for disinfecting water is chlorination. By adding chlorine to drinking water, dangerous microbes such as bacteria, parasites and viruses can be eliminated. [11]

Limitations: Unpleasant taste and odour, formation of harmful disinfection byproducts

1.4.6 Chemical Precipitation

In this method, certain chemicals are added in the medium where the pollutants react with these chemicals and forms the precipitate.[12]

Limitations: Incomplete removal and sludge disposal issues

The traditional methods for wastewater treatment have their own limitations. Hence, it is extremely important to find sustainable process. In the recent advances, Advanced Oxidation Processes (AOPs) using photocatalysis have gained considerable attention due to their significant benefits.[13] Through semiconductor-assisted photocatalysis, freely available solar energy can be converted into usable reactive species and the contaminants can be eliminated. Semiconductor photocatalysis demonstrated several advantages for the removal of organic contaminants compared to the conventional methods including stability, increased degradation efficiency, and the capability of adsorbing a great range of organic and inorganic materials on the photocatalyst surface.[14]

1.5 Catalysis

From the ancient times to the present, catalysis has a wide variety of applications. Catalysis is the process of accelerating the chemical reaction rate by lowering the activation energy barrier. The catalysis process uses the catalyst which helps to alter or speed up the rate of reaction without itself being consumed by the reaction. Hence, the catalyst allows the reaction to proceed much at a much faster rate by providing a lower activation energy alternative pathway for the reaction to occur.[15]

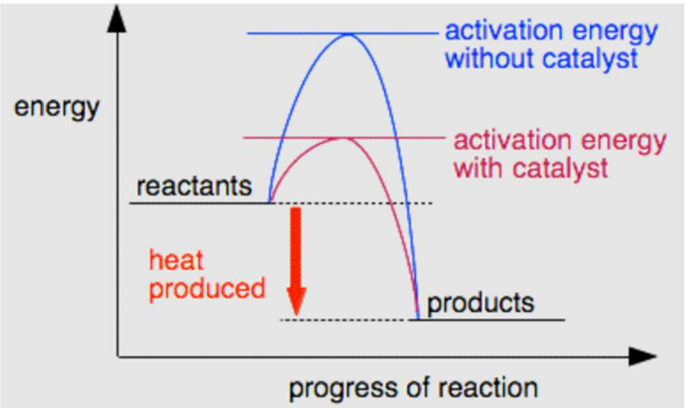

Figure 1.1 Energy transformation diagram for catalysed and non-catalysed reactions

Catalysis is broadly classified into two types depending on the type of phases involved:

1.5.1 Homogeneous catalysis

In this catalytic system, both the reactant and the catalyst are present in the same phase, usually liquid phase. Homogeneous catalysis is used in organic synthesis, polymerization reactions, and various industrial processes.[16]

Example: Esterification of acetic acid with ethanol using sulphuric acid as the catalyst

Limitation: Difficulty in product separation

1.5.2 Heterogeneous catalysis

In this catalytic system, both the catalyst and the reactant are present in different phases.[17]

Example: Haber-Bosch process in the manufacture of ammonia, where the reactants nitrogen and hydrogen are gases and the catalyst iron is present in the solid phase.

Limitation: Cost-effective method

1.6 Photocatalysis

Photocatalysis is the phenomenon in which the catalyst absorbs light and initiates the chemical reaction. On exposure to light, the photocatalyst produces e^- and h^+ in CB and VB respectively. Conduction band is composed of electrons that are present in the innermost shell of the atom and the valence band is an energy band that constitutes

valence electrons which are located on the outermost shell of the atom. The effectiveness of a photocatalyst depends on its tendency to absorb light, generate reactive species and assist the desired chemical transformations having energy equal or higher than bandgap energy.[18] The band gap of the material can be defined as the energy difference between the conduction band and the valence band of that material. Semiconductors function as photocatalysts because they get excited upon exposure to light even at room temperature and produce species which can degrade the contaminants. In environmental remediation, photocatalysis is used an effective approach to remove harmful contaminants from air and water by oxidizing and reducing them into less harmful substances.[19]

1.6.1 Mechanism

The mechanism of photocatalysis can be explained through the following steps:

I. Light Absorption: The photocatalyst absorbs light leading to the excitation of electrons from the valence band to the conduction band.
II. Generation of electron-hole charge carriers: Electron and hole charge carriers are created as a result of this excitation.
III. Migration and surface reactions: On the photocatalyst surface, the electrons and holes move about and take part in redox reactions.
IV. Product Formation: The reaction results in the formation of product such as the decomposed pollutants.

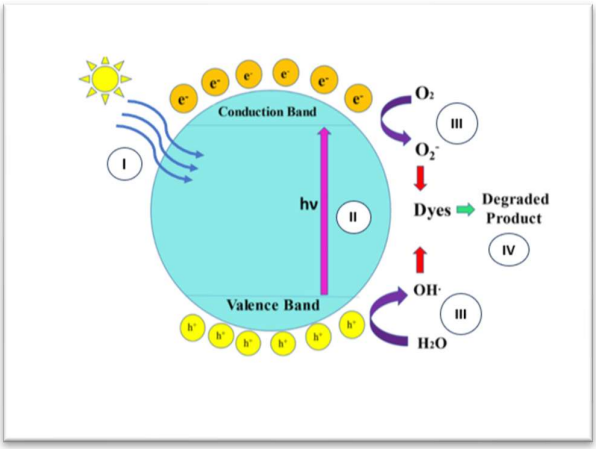

Figure 1.2 Schematic representation of photocatalytic degradation mechanism on a semiconductor surface

Some characteristics of an ideal photocatalyst include includes high surface area, significant visible light absorption ability, appropriate charge transfer, stable for repetitive use, low cost, environment-friendly, and good selectivity towards single product.[20] For high photocatalytic activity, the physiochemical properties of these metal oxides such as size, shape, morphology, composition are taken into account.

In these reactions, oxidative species are generated that are highly reactive (ROS) such as $O_2^{-\bullet}$, H_2O_2 and $OH^{\bullet}$ etc. on the semiconductor surface, which control the oxidation of the surface adsorbed pollutants.

Over the years, photocatalysis has been used in a wide range of applications and as effective approach for environmental remediation. Some applications of photocatalysis include light-driven organic synthesis, pollutant degradation, chromium (VI) reduction, water splitting, nitrogen fixation, etc.

1.6.2 Various semiconducting materials used for photocatalysis

Various materials are used as photocatalysts for environmental cleanup. These materials should possess certain characteristic properties such as high surface area, excellent charge separation, large visible light absorption ability, environment friendly, low cost and stable for repetitive uses.

Metal oxides: These photocatalyst are typically made of semiconducting materials such as TiO_2, Fe_2O_3, ZnO, WO_3. The energy band gap of these materials can be utilized to determine their photocatalytic performance. Metal oxides are generally used for environmental remediation for several years due to their ability to form charge carriers in the presence of light.[21]

Most of the metal oxides have large band gap and are therefore excited by UV light which constitutes over 3-5 percent of the total solar radiation which is not an energy conservative approach. The importance of metal oxide based photocatalyst is attributed to their capability of easy generation of charge carriers on absorption of light, appropriate optical band gap, and high stability. However, there are some limitations of metal oxide based photocatalyst which include photo-induced corrosion and leaching.[22]

Metal sulphides and selenides: The metal sulphides such CdS, MoS, CuS, ZnS and the metal selenides such as CdSe, ZnSe have been used for wastewater treatment using photocatalysis. The metal sulphides are generally used dur to properties like optimal band gap, and appropriate redox potential. However, these photocatalytic materials are vulnerable to photo-corrosion. Hence, these materials cannot be employed for photocatalysis directly.[23]

Carbon-based materials: In the intervening years, carbon-based materials such as graphene, carbon nanotubes (CNTs), fullerenes, graphitic carbon nitride (g-C_3N_4) have acquired considerable attention due to their low cost, earth abundance and high physiochemical activity. The key advantage of these materials is that they do not contain any metal hence there are no chances of metal leaching to take place. However, the limitation of these materials is the high recombination rate of the charge carriers. Carbon nitride which is rich in carbon and nitrogen content and possesses a low band gap energy, is one of the most prominent photocatalyst derived from carbon.[24]

1.7 Graphitic Carbon Nitride: A metal free photocatalyst

C_3N_4 molecules and their precursors can be traced back to 1834, when Berzelius synthesized melon, which is a linear polymer composed of interconnected tri-s-triazine atoms linked by secondary nitrogen atoms, and Liebig gave its name. Graphitic carbon nitride is a metal free photocatalyst composed of nitrogen and carbon atoms. Carbon nitride exists in various allotropic forms which include g-C_3N_4, pseudo cubic C_3N_4, cubic C_3N_4. Among the various allotropes, g-C_3N_4 is considered as one of the most stable form, enriched with high surface morphology and chemically stable in most solvents due to strong van der Waal forces of interaction.

g-C_3N_4 is visible-light active and has a band gap of 2.7eV.[25] Polymeric g-C_3N_4 can be synthesized from any C-rich or N-rich precursor such as melamine, urea, cyanamide, dicyandiamide, etc through calcination in muffle furnace at high temperatures at around 550^{o}C. g-C_3N_4 polymers are yellow-coloured having conduction and valence band energies of -1.1ev and +1.6eV respectively. g-C_3N_4 exhibits an absorption band at approximately 460 nm. Thus, it is a good photocatalyst owing to its desired band gap, which in turn leads to energy conservation. Research

has been carried on the synthesis of g-C_3N_4 and exploring its applications in various fields, including environmental remediation, energy storage, and catalysis.

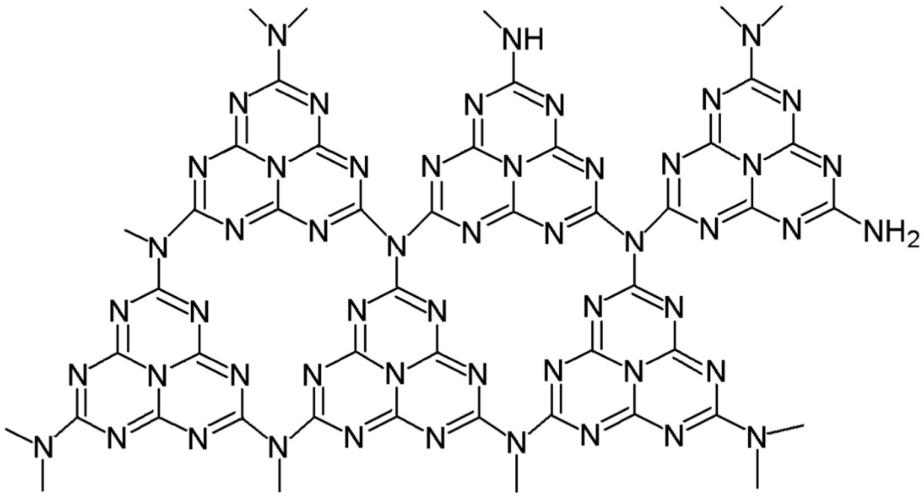

Figure 1.3 Structure of polymeric carbon nitride

1.7.1 Merits of g-C_3N_4

Metal free semiconductor: The g-C_3N_4 is pure carbon-based material which is devoid of any metal atom. This characteristic trait is highly beneficial and protects it from metal leaching.

Optimal bang gap: The g-C_3N_4 acquires low band gap energy of 2.7eV and therefore less energy is required for electron excitation from VB to CB upon light exposure.

Visible light active: The g-C_3N_4 is active in visible light which is naturally available from the sun. Thus, g-C_3N_4 is stable with respect to light.[26]

High Thermal Stability: g-C_3N_4 exhibits excellent thermal stability up to high temperatures around 500^oC thereby enhancing its performance for high temperature applications.

Chemical inertness: g-C_3N_4 possesses a significant feature of chemical inertness which is due to its polymeric conjugated planar structure and does not readily react with any other organic compound.

Insoluble in organic solvents: The compound g-C_3N_4 is insoluble in a diverse range of organic and inorganic solvents.

Non-toxic: g-C_3N_4 is non-hazardous.

Low cost: The various precursors used in the synthesis of g-C_3N_4 have low processing cost and easily available.

1.7.2 Demerits of g-C_3N_4

Low specific surface area: The g-C_3N_4 exhibits an inter-layered structure hence the internal sheets are not efficiently accessible so it leads to minimized surface area.

Reduced surface adsorption: A lower surface area of g-C_3N_4 results in fewer number of surface-active sites for adsorption, which can reduce the overall capability of the material to adsorb the contaminants.

High charge carrier recombination rate: The electrons and holes generated on exposure to light recombine, making the material non-responsive. Due to the rapid recombination capability of these charge carriers, g-C_3N_4 is not suitable for the photocatalytic applications.[27]

1.7.3 Strategies to overcome the limitations of g-C_3N_4

To enhance the photocatalytic performance of g-C_3N_4, various methods are employed which involve formation of composites/heterostructures, nanostructure designing, doping by metals or non-metals, etc. These methods help to enhance the surface area, extend visible light absorption tendency and increase the lifetime of charge carriers.

1.7.3.1 Doping

Doping is the process of adding certain impurities/chemical elements such as metals or non-metals to a semiconductor in order to change its electrical properties. For example, the metal ZrO_2 has a broad band gap, so in order to overcome this limitation, it can be doped with a suitable dopant such as Cu, Co, Fe to adjust the electrical structure, improve photocatalytic activity and increase the tendency to absorb light.[28]

1.7.3.2 Nanostructure Designing

It refers to the process where materials are developed on nanoscale like nanosheets, nanorods, nanotubes.[29] In this method, the bulk materials are converted to nanoscale material using top-down and bottom-up approaches. The properties of the nanomaterial are different from that of the bulk material. In at least one dimension, nanomaterials have structures that range from 1 to 100 nanometers (nm). Their properties are highly influenced by their small size and high surface area-to-volume ratio.

1.7.3.3 Heterostructure Designing/Composite

In this method, composites/heterostructures are prepared by combining photocatalytic materials with other substances to enhance their performance. The composite/heterostructure can be two-component system or multi-composite system. Joining two or more semiconductors elevates the light absorption tendency, enhanced separation of the charges, supresses electron-hole pair recombination rate and boosts the photocatalytic activity.[30] Examples involve TiO_2/g-C_3N_4, ZrO_2/g-C_3N_4.

1.7.3.4 Sensitization

It is a process which requires photo-sensitive dye and a catalyst. Light is absorbed by the dye and electron excitation takes place from the dye's VB to its CB. The reduction reaction occurs on the photocatalyst surface. The application of this method includes photo degradation of harmful dyes such as Rhodamine B, methylene blue.[31]

1.8 Poly (triazine) imide

Crystalline carbon nitrides based on the s-triazine units are emphasized because they allow for a more detailed structural-property studies in comparison to well-known amorphous polymers that contain nitrogen and carbon. Heptazine (1,3,4,6,7,9,9b-heptaazaphenalene, C_6N_7) and the triazine (1,3,5- triazine, C_3N_3) are the two primary foundations of the carbon-nitride materials. The heptazine and triazine units are both aromatic compounds which contain nitrogen and carbon in an alternate fashion. Heptazine and triazine-based compounds are essential precursors and by-products formed from the synthesis of higher molecular weight polymers. Melamine is the most notable of these molecules, the 19^{th} century chemist Justus von Liebig gave it an arbitrary name, and melamine is being used in industry today as an inexpensive

precursor for thermoset plastics and flame-retardants. Poly (triazine) imide, a triazine-based two-dimensional polymer is produced by thermally treating dicyandiamide in eutectic salt melts such as LiX and KX (X= Cl or Br). Fully-delocalized pi-electron systems connected by imide bridges are seen in poly (triazine) imide. Poly (triazine) imide, like melon, has an optical bandgap resulting in encouraging photocatalytic application performance. Because of the strong covalent bonds between individual layers, PTI is one of the very few crystalline carbon nitride materials that can be exfoliated chemically and mechanically into thin layers.[32]

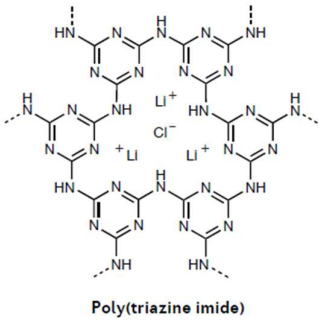

Figure 1.4 Structure of Poly (triazine) imide

1.9 Borophene

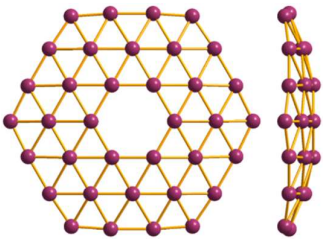

Figure 1.5 Structure of borophene cluster

Boron is an element in the periodic table that is both lightweight and chemically diverse. A two-dimensional (2D) monolayer of elemental boron, borophene has become a fascinating material with exceptional mechanical, chemical, optical, electrical, and catalytic properties.[33] Because of its exceptional qualities, borophene has demonstrated significant promise for a number of innovative uses in the field of sensors, energy storage devices, supercapacitors and medical equipment. In addition

to graphene, borophene is a new class of atom-thick nanomaterials. A two-dimensional carbon allotrope is called graphene which is composed of a single sheet of carbon atoms firmly bonded together in a hexagonal honeycomb lattice. Because graphene lacks a band gap, its application in digital electronics is restricted.[34] The fascinating physical and chemical properties of borophene, such as its exceptional mechanical compatibility, great carrier mobility, promising optical and electrical properties, exceptionally high thermal conductivity, and superb stability, have generated a lot of interest.[35]

1.10 Aims and Objective

Photocatalysts synthesized from certain other materials exhibits various limitations for the environment, therefore environment-friendly materials can prove to be an excellent approach. Carbon-based materials are readily available, non-harmful and safe for the environment. Therefore, the aim and objective of the proposed research work is:

1. To synthesize various PCN based photocatalyst
2. To characterize the photocatalysts for its structural, optical and morphological studies.
3. To study the photocatalytic activity of developed catalyst towards degradation of Rhodamine B dye and Chromium (VI) reduction
4. To understand the mechanistic aspect towards the photocatalytic degradation of Rhodamine B and Chromium (VI) reduction

1.11 Overview of Thesis

There are four chapters in this thesis, which includes an introduction, materials and methods, result and discussion, and conclusion.

Chapter-1 Introduction: This includes various environmental issues, photocatalysis and its mechanism, different semiconductor photocatalysts for dye degradation and chromium (VI) reduction.

Chapter-2 Synthesis and characterization methods: This includes materials used in this work, method adopted to synthesize the materials, and the characterization techniques used to investigate various properties.

Chapter-3 Results and discussion: This chapter focuses on the various aspects such as the structure, optical properties of the synthesized materials, and the photocatalytic activity of Rhodamine B dye and Chromium (VI) reduction.

Chapter-4 Summary, conclusion and future prospects: This provides a brief summary of the proposed work, conclusion and future scope.

1.12 References

1. Arif, A., et al., *3. Water pollution and industries.* Pure and Applied Biology (PAB), 2020. **9**(4): p. 2214-2224.
2. Sanusi, I.O., et al., *Occurrence, environmental impact and fate of pharmaceuticals in groundwater and surface water: a critical review.* Environmental Science and Pollution Research, 2023. **30**(39): p. 90595-90614.
3. Jagaba, A.H., et al., *Sources of water contamination by heavy metals*, in *Membrane technologies for heavy metal removal from water*. 2024, CRC Press. p. 3-27.
4. Sharma, P., S. Tripathi, and R. Chandra, *Phytoremediation potential of heavy metal accumulator plants for waste management in the pulp and paper industry.* Heliyon, 2020. **6**(7).
5. Jacobs, J.A. and S.M. Testa, *Overview of chromium (VI) in the environment: background and history.* Chromium (VI) handbook, 2005: p. 1-21.
6. Saha, R., R. Nandi, and B. Saha, *Sources and toxicity of hexavalent chromium.* Journal of Coordination Chemistry, 2011. **64**(10): p. 1782-1806.
7. Ighalo, J.O., et al., *Cost of adsorbent preparation and usage in wastewater treatment: a review.* Cleaner Chemical Engineering, 2022. **3**: p. 100042.
8. Zubair, M.M., H. Saleem, and S.J. Zaidi, *Recent progress in reverse osmosis modeling: An overview.* Desalination, 2023. **564**: p. 116705.
9. Ateia, M., C. Yoshimura, and M. Nasr, *In-situ biological water treatment technologies for environmental remediation: a review.* J Bioremed Biodeg, 2016. **7**(348): p. 2.
10. Panizza, M. and G. Cerisola, *Direct and mediated anodic oxidation of organic pollutants.* Chemical reviews, 2009. **109**(12): p. 6541-6569.
11. Huang, B., et al., *Chlorinated volatile organic compounds (Cl-VOCs) in environment—sources, potential human health impacts, and current remediation technologies.* Environment international, 2014. **71**: p. 118-138.
12. Saravanan, A., et al., *Effective water/wastewater treatment methodologies for toxic pollutants removal: Processes and applications towards sustainable development.* Chemosphere, 2021. **280**: p. 130595.
13. Saravanan, A., et al., *A detailed review on advanced oxidation process in treatment of wastewater: Mechanism, challenges and future outlook.* Chemosphere, 2022. **308**: p. 136524.
14. Yang, X. and D. Wang, *Photocatalysis: from fundamental principles to materials and applications.* ACS Applied Energy Materials, 2018. **1**(12): p. 6657-6693.
15. Lin, L., et al., *Emerging heterogeneous catalysts for biomass conversion: studies of the reaction mechanism.* Chemical Society Reviews, 2021. **50**(20): p. 11270-11292.
16. Kumar, A., P. Daw, and D. Milstein, *Homogeneous catalysis for sustainable energy: hydrogen and methanol economies, fuels from biomass, and related topics.* Chemical reviews, 2021. **122**(1): p. 385-441.
17. Vogt, C. and B.M. Weckhuysen, *The concept of active site in heterogeneous catalysis.* Nature Reviews Chemistry, 2022. **6**(2): p. 89-111.
18. Banerjee, T., et al., *Polymer photocatalysts for solar-to-chemical energy conversion.* Nature Reviews Materials, 2021. **6**(2): p. 168-190.
19. Melchionna, M. and P. Fornasiero, *Updates on the Roadmap for Photocatalysis.* Acs Catalysis, 2020. **10**(10): p. 5493-5501.
20. Wen, J., et al., *A review on g-C3N4-based photocatalysts.* Applied surface science, 2017. **391**: p. 72-123.

21. Krishnan, A., et al., *A review on transition metal oxides based photocatalysts for degradation of synthetic organic pollutants.* Journal of Environmental Sciences, 2024. **139**: p. 389-417.
22. Khan, M.M., S.F. Adil, and A. Al-Mayouf, *Metal oxides as photocatalysts*. 2015, Elsevier. p. 462-464.
23. Ayodhya, D. and G. Veerabhadram, *A review on recent advances in photodegradation of dyes using doped and heterojunction based semiconductor metal sulfide nanostructures for environmental protection.* Materials today energy, 2018. **9**: p. 83-113.
24. Cao, S., et al., *Polymeric photocatalysts based on graphitic carbon nitride.* Advanced Materials, 2015. **27**(13): p. 2150-2176.
25. Kessler, F.K., et al., *Functional carbon nitride materials—design strategies for electrochemical devices.* Nature Reviews Materials, 2017. **2**(6): p. 1-17.
26. Zhang, M., et al., *A critical review of g-C3N4-based photocatalytic membrane for water purification.* Chemical Engineering Journal, 2021. **412**: p. 128663.
27. Pattanayak, D.S., et al., *Noble metal–free doped graphitic carbon nitride (g-C3N4) for efficient photodegradation of antibiotics: progress, limitations, and future directions.* Environmental Science and Pollution Research, 2023. **30**(10): p. 25546-25558.
28. Sharaf, I.M., et al., *Unraveling the effect of Cu doping on the structural and morphological properties and photocatalytic activity of ZrO2.* Heliyon, 2024. **10**(1).
29. Wang, X., et al., *One-dimensional titanium dioxide nanomaterials: nanowires, nanorods, and nanobelts.* Chemical reviews, 2014. **114**(19): p. 9346-9384.
30. Fathy, A., *Investigation on microstructure and properties of Cu-ZrO2 nanocomposites synthesized by in situ processing.* Materials Letters, 2018. **213**: p. 95-99.
31. Le, T.T., et al., *Water splitting on Rhodamine-B dye sensitized Co-doped TiO2 catalyst under visible light.* Applied Catalysis B: Environmental, 2012. **111**: p. 397-401.
32. Sun, J., et al., *Poly (triazine imide) ligand based 2D metal coordination polymers: Design, synthesis and application in electrocatalytic water oxidation.* Electrochimica Acta, 2022. **401**: p. 139463.
33. Rahman, A., et al., *Emerging 2D borophene: synthesis, characterization, and sensing applications.* Sensors and Actuators A: Physical, 2023. **359**: p. 114468.
34. Kistanov, A.A., et al., *Exploring the charge localization and band gap opening of borophene: a first-principles study.* Nanoscale, 2018. **10**(3): p. 1403-1410.
35. Wang, Z.-Q., et al., *Band structure engineering of borophane by first principles calculations.* RSC Advances, 2017. **7**(75): p. 47746-47752.

CHAPTER 2

SYNTHESIS AND CHARACTERIZATION METHODS

The aim of this chapter is to discuss the method of synthesis, details of the characterization techniques along with their principle and method involved in measurement of photocatalytic activity of the prepared heterostructure 5(0.5B-PTI)-PCN.

2.1 Chemicals

For the current study, urea (99.5%), melamine (99%), methanol (99.9%), lithium chloride, boron, acetone (99%), Rhodamine B dye, potassium dichromate, diphenylcarbonohydrazide (DPC), sulphuric acid were purchased from Merck, India. All reagents were used without further purification as provided.

2.2 Methods of Preparation

2.2.1 Preparation of PCN

Polymeric carbon nitride was prepared from melamine and urea using calcination process.[1] 10 gm urea and 1 gm melamine were mixed in a mortar - pestle, transferred in a silica crucible, it was covered with lid and heated at 550^{o}C for 2 hours in a muffle furnace, resulting in yellow powder that was labelled as PCN.

2.2.2 Preparation of borophene/Exfoliation of Boron

For exfoliation of borophene, 50 mg of boron was dispersed in 40 mL of acetone, ultrasonicated for 12 hours. The dispersion was then centrifuged at 5000 r.pm. The borophene so obtained was separated and dried in a petridish.

2.2.3 Preparation of PTI

PTI was prepared from melamine and lithium chloride using calcination process.10 gm melamine and 1gm lithium chloride were taken in a silica crucible, it was covered with lid and calcined at 600^{o}C for 2 hours. The product obtained was washed with distilled water, dried in an oven at 60^{o}C for 12 hours, resulting in yellowish powder that was labelled as PTI.

2.2.4 Preparation of B-PTI

For the preparation of B-PTI composite, 200 mg PTI was dispersed in 40 mL acetone, sonicated in an ultra-sonicator for 4 hours to obtain exfoliate PTI was obtained. Further 0.5 mg borophene was dispersed in 20 mL ethylene glycol, and sonicated for 4 hours and the exfoliated boron dispersion was obtained. The exfoliated boron dispersion and exfoliated PTI dispersion were then mixed together, stirred for 12 h, centrifuged and washed 3 times with acetone. The obtained xB-PTI composite was dried overnight at 60^{o}C in an oven. By varying the amount of borophene, different xB-PTI composites were prepared. The amount of borophene (x) varied as 1mg, 0.5mg, 0.25mg and the various B-PTI composites obtained were 1B-PTI, 0.5B-PTI and 0.25B-PTI. From the various B-PTI composites that were synthesized, 0.5B-PTI was the optimized composite due to its maximum dye degradation tendency. Hence, 0.5B-PTI composite was further used to synthesize the binary heterostructure (0.5B-PTI)-PCN where borophene acts as a mediator.

2.2.5 Preparation of (B-PTI)-PCN Heterostructure

For the preparation of x(B-PTI)-PCN composite, 200 mg PCN was dispersed in 50 mL methanol, sonicated for 2 hours and the suspension of PCN was obtained. 10 mg (5%) of 0.5B-PTI was mixed with a PCN suspension and stirred for 2 h on the magnetic stirrer at 60^{o}C. The solvent was allowed to evaporate till dryness to obtain 5(0.5B-PTI)-PCN heterostructure. By varying the amount of 0.5B-PTI, different x(0.5B-PTI)-PCN heterostructures were synthesized. The amount of 0.5B-PTI(x) varied as 40mg, 20mg, 10mg, 5mg and 2mg and the various (0.5B-PTI)-PCN heterostructures obtained were 20(0.5B-PTI)-PCN, 10(0.5B-PTI)-PCN, 5(0.5B-PTI)-PCN, 2.5(0.5B-PTI)-PCN and 1(0.5B-PTI)-PCN, respectively. From the various x(0.5B-PTI)-PCN heterostructures that were synthesized, 5(0.5B-PTI)-PCN was the optimized binary heterostructure due to its maximum dye degradation efficiency. Hence, in the optimized 5(0.5B-PTI)-PCN binary heterostructure, borophene acts as a mediator between PCN and PTI and allows for the better charge transfer.

2.3 Characterization Techniques

2.3.1 Powder X-ray Characterization

Powder X-ray diffraction (P-XRD) provides information about the crystal structure, interplanar distance and lattice parameters of solid powder samples. In this technique,

the sample is exposed to an X-ray beam and diffraction patterns with varying angles of incidence was recorded.[2] Both angle and pattern are determined by the diffracted strength. The whole assembly is comprised of an X-ray source with wavelength ranging from 0.7 to 2 A^o, collimators and the detector. X-ray diffraction is based on the Bragg's equation which can be explained as follows:

$n \lambda = 2d \sin \theta$……. (1)

where, n = order of diffraction (1,2,3, …), λ = wavelength of X-ray, d = interplanar distance between crystalline planes, θ = angle of incidence of X-ray

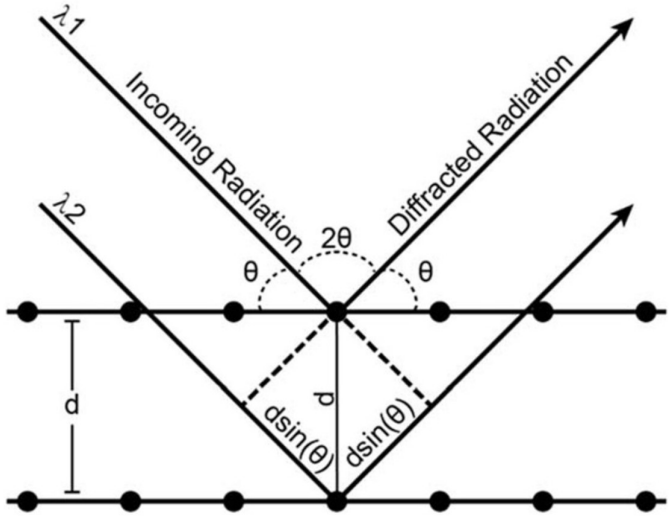

Figure 2.1 Representation of Bragg's diffraction in crystal structure

A plot of diffracted ray intensity versus diffraction angle 2 θ gives a unique pattern, with a corresponding set of planes. The most important application of Scherrer's equation is in X-ray diffraction (XRD), which uses the broadening of diffraction peaks to estimate a material's crystallite size.

The Scherrer's equation can be explained as follows:

$D = K\lambda / \beta \cos \theta$……. (2)

(where, D is the crystallite size in A^o, K = 0.9 is Scherrer's constant, λ is the wavelength of X-ray in A^o, β is the full width at half maximum (FWHM) of the peak (in radians), θ = incident angle or Bragg's angle

2.3.2 UV-Visible Spectroscopy

The UV-Vis spectroscopy is a technique that is used to determine the concentration of known solutes in solution through a measurement of quantitative measurement. UV-Vis spectroscopy is governed by the Beer-Lambert law. According to this law, the amount of light absorbed by a solution is directly proportional to the concentration of the absorbing species and the path length through which light travels from the solution. In UV-Vis spectroscopy, the amount of light absorbed by the sample at a specific wavelength can be determined by comparing the incident radiation (I_o) and the transmitted radiation (I_t). This absorption can be used to evaluate known solute concentrations based on Beer-Lambert law.

$$A = \log (I_o/I_t) * 100 = \varepsilon cl \ldots\ldots\ldots\ldots\ldots\ldots\ldots\ldots (3)$$

Where, A = absorbance, ε = molar excitation coefficient, c = concentration of the species, l = thickness of the sample holder

As the UV-Vis light passes through the sample, some of it is absorbed while some part is transmitted. When a sample comes in contact with visible or UV light: after absorbing energy, the electronic transition takes place from the ground state, which has a lower energy to the excited state, which has a higher energy. The wavelength of light that is absorbed is determined by the energy difference between these orbitals. For analysis UV-Visible spectrophotometer (UV-1800) Shimadzu was used.

2.3.3 UV-Vis Diffuse Reflectance Spectroscopy

Diffuse reflectance spectroscopy (DRS) is an analytical technique used for analyzing the optical properties of powders, rough surfaces, or opaque materials. By examining how a material absorbs light close to the absorption edge UV-Vis Diffuse Reflectance spectroscopy (UV-DRS) can determine the optical bandgap of a material, particularly semiconductors. UV-DRS functions by scattering and diffusing UV-visible light when it strikes a powdered or opaque solid sample.[3] This reflected light is gathered and analyzed to estimate the amount of light absorbed by the substance. The Kubelka-

Munk function is used to convert the reflectance data into a form proportional to absorbance, which is then used to study the electronic transitions and evaluate the optical band gap in solid materials. The UV-DRS method uses barium sulphate ($BaSO_4$) as a standard reference material. The samples are evenly transferred into the sample holders and the UV-DRS spectra of the specimen are obtained by striking the sample with varying frequency of light. In the UV-DRS plot, the x-axis represents the photon energy ($h\upsilon$) in electron-volts (eV) which is calculated from the wavelength of light, while the y-axis represents $[F(R).h\upsilon]^n$ where F(R) is the Kubelka-Munk function derived from reflectance data and 'n' depends on the type of electronic transition – ½ for direct and 2 for indirect transitions. Optical absorption of the catalysts was measured on ultraviolet-visible diffuse reflectance spectrophotometer (UV-Vis) DRS on UV-2600 Shimadzu Japan.

2.3.4 Fourier Transform Infrared Spectroscopy (FT-IR)

FT-IR is an advanced technique used to determine the presence of various functional groups present in the sample. FT-IR measures a material's absorption of infrared light at different wavelengths to produce an infrared spectrum of that material. Unlike IR spectroscopy, FT-IR uses an interferometer to gather all wavelength data simultaneously. The raw signal so obtained is then transformed into a readable spectrum using a Fourier transform. This technique helps to identify functional groups, chemical bonds, and material composition in solids, by enabling a higher resolution, quicker and more precise determination of molecular vibrations. An FT-IR spectrum normally covers the mid infrared region, which is particularly important for identifying chemical vibrations and functional groups, between 4000 and 400 cm^{-1}. The fingerprint area (1500 – 400 cm^{-1}) which contains complex absorption patterns particular to each molecule, and the functional group region (4000 – 1500 cm^{-1}) where the presence of strong peaks identify particular bond types like O-H, N-H, and C=O are two important absorption zones included in this range. Because of its wide spectrum range, FT-IR provides structural details on both organic and inorganic compounds. FTIR spectra were recorded on Nicolet iS50 FTIR spectrometer (Thermo Fischer Scientific, USA) using KBr pellet technique.

2.3.5 Surface area and pore size distribution

Surface area and porosity are important characteristics in the field of catalysts design and heterogeneous catalysis. Since total surface area affects accessibility to the active site and is thus frequently linked to catalytic activity, it is a crucial component of solid catalyst performance. The Brunauer-Emmett-Teller (BET) technique can be applied to nitrogen adsorption isotherms to determine the surface area and pore size of powder and porous materials.[4] The degree of gas adsorption rises with increasing pressure and is proportional to the relative pressure. The BET analysis makes the assumption that adsorption takes place on a free surface at saturation pressure and that is accomplished by creating multiple adsorbed layers with an infinite number of adsorbed layers. The Langmuir adsorption isotherm is the model that corresponds to the maximum adsorption and is represented by monolayer adsorption.

$C_e/ q_e = 1/ q_{max} K_L + C_e/ q_{max}$……. (4)

Where, q_e = amount of adsorbate adsorbed per unit mass of adsorbent at equilibrium (mg/g)

C_e = equilibrium concentration of adsorbate in solution (mg/L)

K_L = Langmuir constant related to the affinity of binding sites (L/mg)

To determine the surface area and pore size of the catalyst, Qunatachrome Nova touch 1, BET surface area analyzer was used.

2.3.6 High-Resolution Transmission Electron Microscopy (HR-TEM)

High-Resolution Transmission Electron Microscopy (HR-TEM) is a sophisticated imaging technique that provides sub-nanometer to atomic resolution views of a material's atomic structure. HR-TEM enables the direct visualization of lattice fringes, grain boundaries, defects, and crystal structures in solids. [5] A high-energy electron beam (usually 200-300 keV) is passed through an ultrathin sample in HR-TEM, where electrons interact with the material’s atomic structure. Because of phase variations, the atoms scatter the electrons, as they travel through, creating interference patterns. Lattice fringes, crystal planes, and structural defects can be examined at the nanoscale through atomic-scale resolution photographs created by magnifying and recording these patterns.

2.3.7 Evaluation of Photocatalytic Activity

The photocatalytic activity of the various catalyst is evaluated for Rhodamine B dye degradation and Cr (VI) reduction.[6] The photo-reactor is equipped with a light source, a magnetic stirrer, a fan and a sample container. The sample vessel (a 250 mL beaker with glass lid) is put over the magnetic stirrer which is surrounded by 10 fluorescent bulbs (each 100W). To avoid excess heat generation by the lamps during the reaction, the entire equipment is housed in a rectangular chamber with a fan.

For the analysis of Rhodamine B dye degradation, 35 mg of the catalyst 5(0.5B-PTI)-PCN was mixed with 35 mL of RhB (20mg/L) in a 250 mL beaker. The reaction mixture was stirred for 30 minutes to establish adsorption-desorption equilibrium before light irradiation. During light irradiation, 5 mL sample aliquots were collected at the time interval of 5 minutes each and centrifuged. The change in concentration of RhB dye was measured using (UV 1800 Shimadzu) UV-Vis spectrophotometer, where absorbance values of each sample were recorded and the degradation efficiency was calculated by the formula:

Degradation (%) = $(C_0-C_t)/C_0 * 100$……. (5)

(where, C_0 is the initial concentration of the dye, C_t = concentration at a particular time)

50 mg catalyst was taken in 50 mL $K_2Cr_2O_7$ solution (20 mg/L). 19.7 mg citric acid was added to it. The reaction mixture was stirred for 30 minutes to establish adsorption-desorption equilibrium before light irradiation. During light irradiation 5 mL sample aliquots was withdrawn, it was filtered through a filter syringe, collected at 5 minutes interval and change in concentration of Cr was measured using (UV 1800 Shimadzu) UV-Vis spectrophotometer.

Now, separate storage vials (glass vials) were taken and 7mL (0.2M) H_2SO_4 was added in each vial. 0.2 mL of 1,5 diphenylcarbonohydrazide (DPC) solution was added into the storage glass vials (which already had 7 mL H_2SO_4) and shaken for proper mixing. 2 mL of Chromium (VI) aliquots was added into the storage glass vials and the violet-coloured complex was formed. The vials were kept for 10 minutes for proper complex formation. Then, the absorbance data of the prepared solution was assessed using a (UV 1800 Shimadzu) UV-Vis spectrophotometer where absorbance values of each sample were recorded and the reduction efficiency was calculated by the formula:

Reduction (%) = $(C_0-C_t)/C_0 * 100$……. (6)

(where, C_0 is the initial concentration of Cr (VI), C_t = concentration at a particular time)

2.4 References

1. Wirnhier, E.A., *Solvothermal and Ionothermal Approaches to Carbon Nitride Chemistry*. 2013, lmu.
2. Pecharsky, V.K. and P.Y. Zavalij, *Fundamentals of powder diffraction and structural characterization of materials*. 2009: Springer.
   Rocha, F.S., et al., *Experimental methods in chemical engineering: Ultraviolet visible spectroscopy—UV-Vis.* The Canadian Journal of Chemical Engineering, 2018. **96**(12): p. 2512-2517.
3. Kortüm, G., W. Braun, and G. Herzog, *Principles and techniques of diffuse-reflectance spectroscopy.* Angewandte Chemie International Edition in English, 1963. **2**(7): p. 333-341.
4. Peyravi, A., et al., *Porous carbon black-polymer composites for volatile organic compound adsorption and efficient microwave-assisted desorption.* Journal of Colloid and Interface Science, 2022. **612**: p. 181-193.
5. Lin, Y., et al., *Analytical transmission electron microscopy for emerging advanced materials.* Matter, 2021. **4**(7): p. 2309-2339.
6. Laouini, S., A. Bouafia, and M. Tedjani, *Catalytic activity for dye degradation and characterization of silver/silver oxide nanoparticles green synthesized by aqueous leaves extract of Phoenix dactylifera L.* 2021.

CHAPTER 3

RESULTS AND DISCUSSION

This chapter discusses about the results and conclusions of various experiments and characterization methods, including phase identification, surface area analysis, optical properties, recyclable nature, quencher study and photocatalytic performance of synthesized composites towards RhB dye degradation and Cr (VI) reduction.

3.1 Crystal Structure, Phase, and Structural Analysis

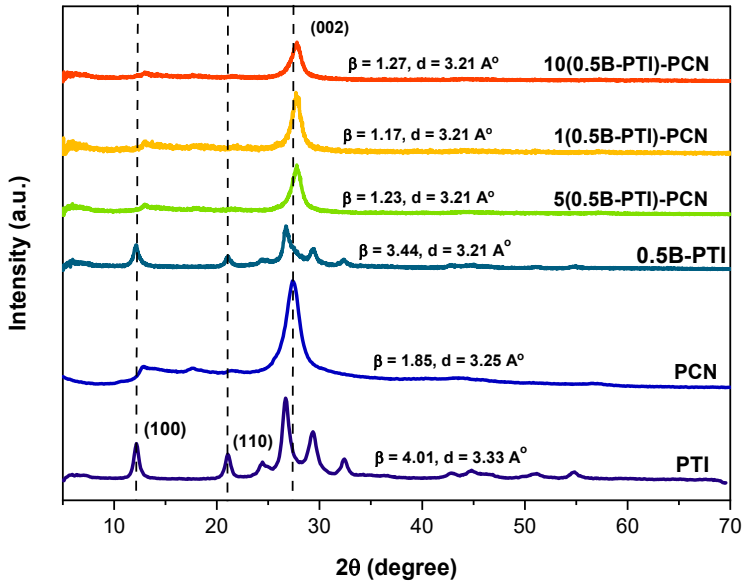

Figure 3.1 XRD pattern of various catalysts

The crystal structure and phase of the various composites were examined using powder X-ray diffraction (P-XRD). From the XRD pattern, (Figure 3.1) it was observed that PCN showed two clear diffraction peaks at 27.3° and 13.1° 2θ angles corresponding to the (002) and (100) planes respectively.[1] Whereas PTI showed the diffraction peaks at 12.2°, 21.1°, 26.6° and 29.3° 2θ angles corresponding to (100), (110), (002), (102) planes respectively.[2] The full width at half maximum (FWHM) values of PCN, PTI, 0.5B-PTI, 1(0.5B-PTI)-PCN, 5(0.5B-PTI)-PCN and 10(0.5B-PTI)-PCN were found to be 1.85, 4.01, 3.44, 1.17, 1.23 and 1.27 respectively. Comparing the XRD patterns of PCN and PTI sample have distinct diffraction patterns, PTI shows sharp and intense diffraction peaks indicating different crystalline structures. 0.5B-PTI

resembles diffraction peak similar to PTI but the peaks are less sharp which indicates the amorphous nature of 0.5B-PTI. In various x(0.5B-PTI)-PCN composites, the FWHM value is increasing as the amount of 0.5B-PTI increases in the composite and the peak corresponding to (002) plane is getting broader and less sharper indicating reduction in crystallinity.

In PCN, the interlayer spacing (d-spacing) corresponding to 27.3° peak is calculated to be approximately 3.25 A°, depicting a 2D graphite-like layered structure. The d-spacing for 26.6° peak in PTI was evaluated to be 3.33A°. As compared to PCN, the interlayered spacing of PTI get increased from 3.25 to 3.33 A° due to the intercalation of ions in PTI. In case of the composites, 1(0.5B-PTI)-PCN, 5(0.5B-PTI)-PCN, 10(0.5B-PTI)-PCN all show a d-spacing of 3.21A° corresponding to (002) plane, which is much closer to pure PCN (3.25A°) than to pure PTI (3.33 A°). This suggests that PCN remains the dominant structural framework in the composites even with increasing 0.5B-PTI content. A reduction in interlayer spacing to 3.21 A° in composites indicates that the layers are packing more tightly in the composites than in either of the base materials. Another reason for this reduced spacing can be attributed to the improved layer stacking which occurs due to the incorporation of 0.5B-PTI which promotes the better ordering of the PCN layers, reducing structural defects or interlayer distortions. The incorporation of 0.5B-PTI into PCN matrix enhances the interlayer packing and leads to the reduction in the structural defects.

3.2 FT-IR (Fourier Transform Infrared Spectroscopy)

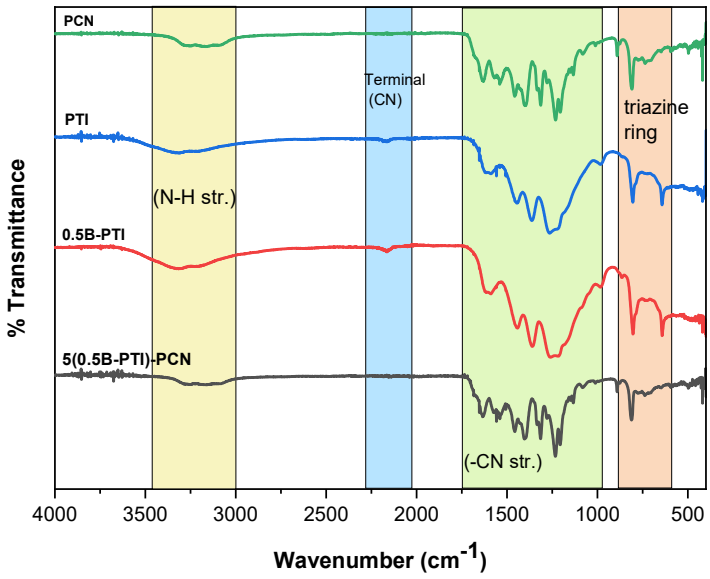

Figure 3.2 FT-IR spectra of PCN, PTI, 0.5B-PTI and 5(0.5B-PTI-PCN)

The structural features of the prepared catalysts were analysed using Fourier Transform Infrared Spectroscopy (FT-IR) to provide detailed information. From the FT-IR spectra, PCN shows a significant peak at 2200 cm^{-1} which corresponds to the stretching vibration of the terminal nitrile group (-CN).[3] The peak at 808 cm^{-1} in PCN, PTI, 0.5B-PTI and 5(0.5B-PTI)-PCN arises from the out-of-plane ring bending mode of C-N heterocycles in both triazine and heptazine units, while the strong absorption peak at 1150-1750 cm^{-1} is caused by the stretching vibration mode of the aromatic (-CN). Additionally, a comparatively weak absorption peak at 2175 cm^{-1} is observed corresponding to the stretching vibration of cyano units (C≡N). The broad peak ranging between 3000-3400 cm^{-1} corresponds to the N-H stretching mode.

The peak at 650 cm^{-1} in FT-IR observed in PTI but absent in PCN suggests the presence of a vibration mode unique to PTI's structure. The peak at 650 cm^{-1} in PTI is generally attributed to the out-of-plane bending vibrations associated with imide bridging units (-NH- or -N=) in PTI's layered ionic framework and crystalline nature of PTI compared to PCN. PCN is heptazine-based framework with a more disordered, non-ionic structure and lacks the planar imide linkages and crystalline order that give rise to the specific lattice or

out-of-plane vibrations seen in PTI. The optimized heterostructure 5(0.5B-PTI)-PCN, shows the characteristic peaks of both PCN and PTI but lacks the peak at 650cm^{-1} which may be due to less amount of PTI in the 5(0.5B-PTI)-PCN composite and PTI is present in very less amount hence the signal might be too weak to be detected.

3.3 Optical Property and Charge Separation Efficiency

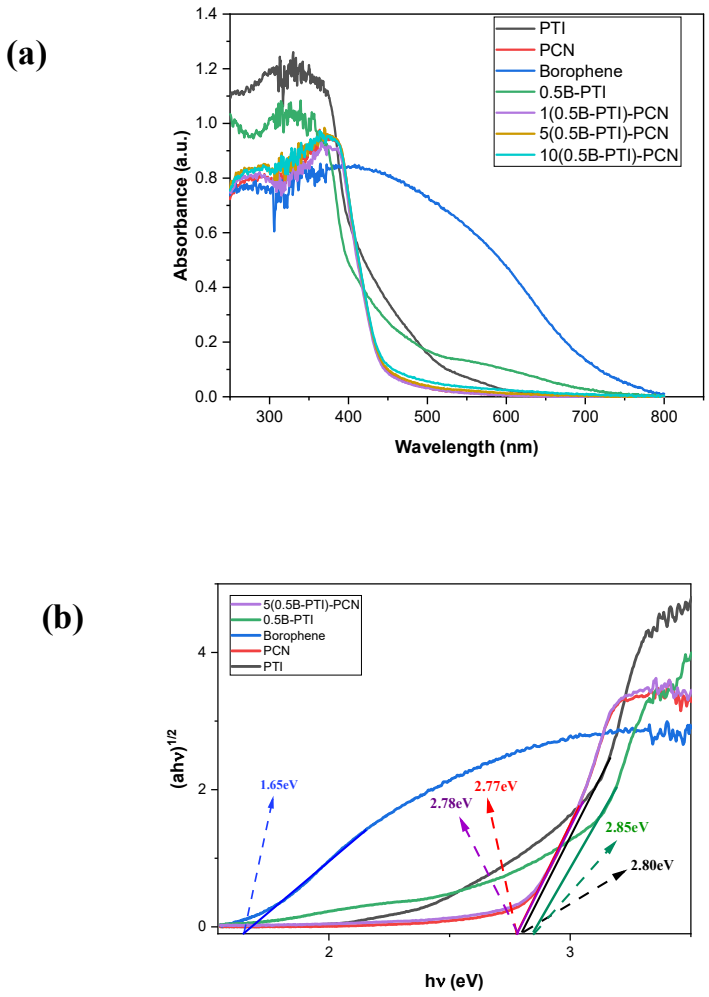

Figure 3.3 (a) UV-Visible diffuse reflectance spectra and (b) Kubelka-Munk plot of various catalysts

The UV-Vis diffuse reflectance spectroscopy (UV-Vis DRS) spectra were utilized to evaluate the optical properties of the synthesized catalyst. Upon exposure to UV-Visible light the catalysts' responses were recorded. Analysis of the spectra revealed

that PCN and PTI exhibit optical activity in the visible range with a maximum absorption edge around 450 nm and 525 nm respectively, which corresponds to the visible portion of the electromagnetic spectrum. The band gap of the catalysts were determined using Kubelka-Munk (KM) plot by plotting the square root of the direct bandgap function $(ah\upsilon)^{1/2}$ against photon energy ($h\upsilon$).[4] From the KM plot the bandgap of borophene, PCN, PTI, 0.5B-PTI and 5(0.5B-PTI)-PCN was found to be 1.65, 2.77, 2.80, 2.85, and 2.78 eV respectively.

For 5(0.5B-PTI)-PCN, the band gap is 2.78 eV, indicating that the heterostructure band gap value falls between those of PCN and PTI.

3.4 High-Resolution Transmission Electron Microscopy (HR-TEM)

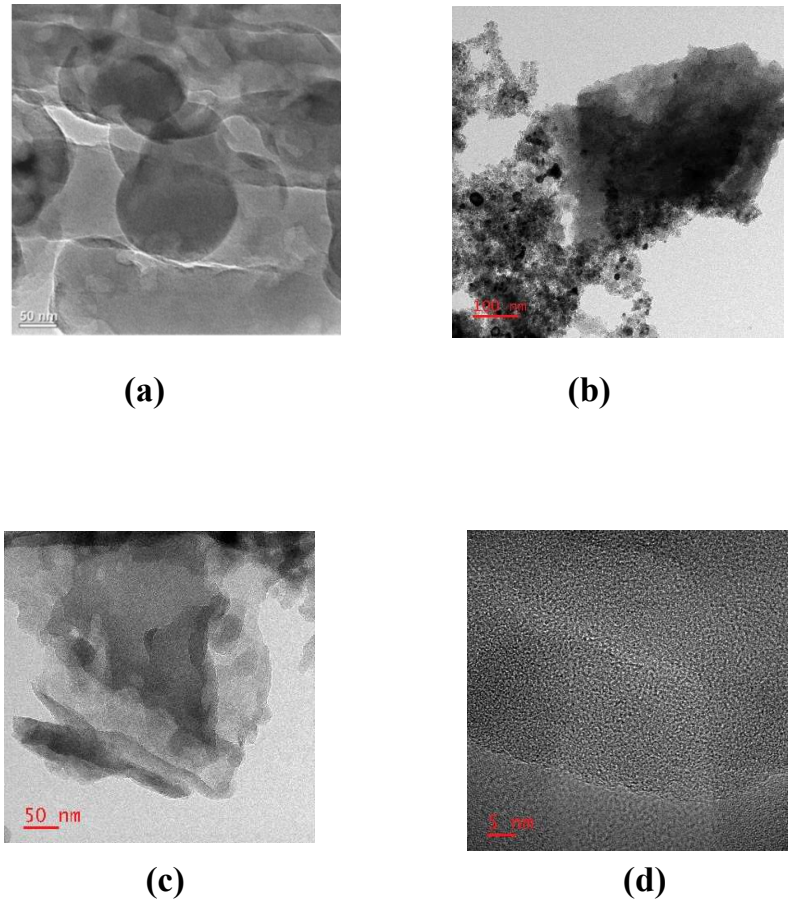

Figure 3.4 TEM images of (a) PCN (b) PTI (c) and (d) 5(0.5B-PTI)-PCN

High-Resolution Transmission electron microscopy (TEM) was employed to investigate the structural and morphological characteristics of 5(0.5B-PTI)-PCN. The image (c) showing 5(0.5B-PTI)-PCN reveals sheet-like, layered structure with curved surface, which are characteristic of polymeric carbon nitride (PCN) material as shown in figure 3.4 (a). In figure 3.4(b), PTI being crystalline in nature depicts a layered morphology demonstrating the 2D-sheets. The current variation indicated different thickness or overlapping layers, suggesting the composite has a 2D-like nanosheet structure. While the B-PTI component may not be individually resolved at this magnification, its presence within the PCN matrix could be inferred by slight contrast differences or embedded darker regions, illustrating heterogenous integration. The material shown in figure (d) is 5(0.5B-PTI)-PCN. The uniform grainly texture across the image suggests a well-dispersed and amorphous to semi-crystalline structure, typical for PCN-based materials. There is no clear lattice fringe over large areas, which indicates that the material is mostly amorphous or has disordered layered structure with few crystalline domains. The bottom left appears to show a layered or sheet-like formation, which could correspond to stacked layers of PCN or PTI nanosheets.

3.5 Surface area and pore size distribution

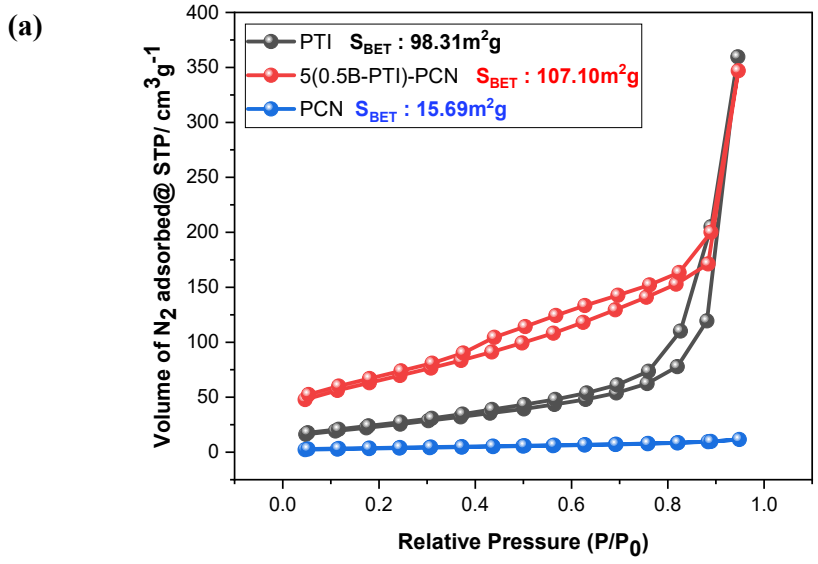

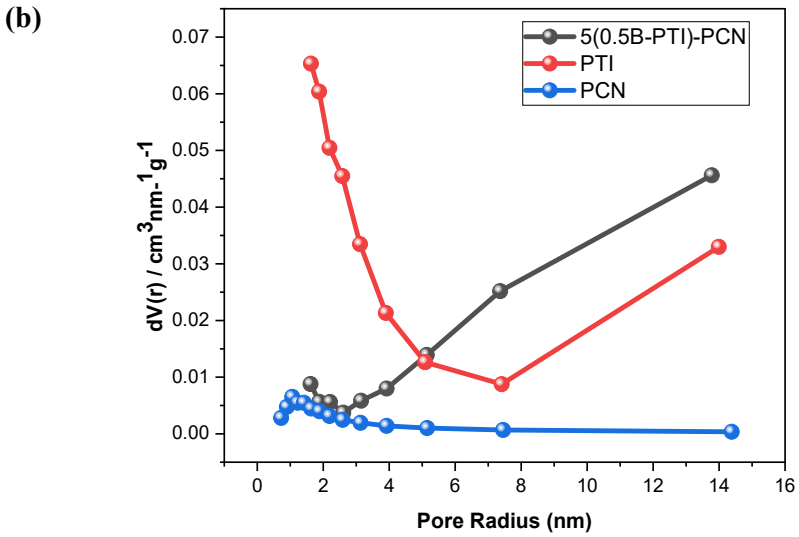

Figure 3.5 (a) N_2 adsorption-desorption isotherm and (b) pore size distribution of PCN, PTI and 5(0.5B-PTI)-PCN

Table No. 3.1 Surface and structural Properties of catalysts

Sample	S_{BET} (m^2/g)	Pore radius (nm)	Pore Volume (cm^3/g)
PCN	15.6	1.06	0.018
PTI	98.3	1.62	0.234
5(0.5B-PTI)-PCN	107.1	13.7	0.564

The surface area and pore size of the synthesized catalyst were evaluated using nitrogen adsorption-desorption isotherms. PCN and PTI showed a Brunauer-Emmett-Teller (BET) surface area of 15.6 m^2/g and 98.3m^2/g respectively, which increased to 107.1 m^2/g for the 5(0.5B-PTI)-PCN heterostructure. Moreover, the pore volume of PCN and PTI were found to be 0.018 cm^3/g and 0.234 cm^3/g respectively whereas the 5(0.5B-PTI)-PCN shows higher pore volume to 0.564 cm^3/g. The surface area increases significantly from PCN to PTI and even more in the composite 5(0.5B-PTI)-PCN, suggesting structural modifications that enhance porosity exfoliation.

The high surface area in 5(0.5B-PTI)-PCN indicates higher pore sizes, thus improving adsorption or catalytic performance. The trend in surface area correlates with improved

functional performance, since high surface area often enhances active site availability. Therefore, increase in surface area after composite formation results in increased number of surface-active sites and greater photocatalytic performance.

The pore radius of pristine materials PCN and PTI are 1.06 nm and 1.62 nm respectively whereas the pore radius of 5(0.5B-PTI)-PCN is 13.7 nm. The composite 5(0.5B-PTI)-PCN exhibits mesoporous structure (pore size >2 nm) compared to microporous PCN and PTI (<2 nm). This increase in pore radius suggests that there is interlayer expansion with improved diffusion having more accessible active sites. This large pore radius (13.77 nm) in the composite suggests that doping of borophene in PTI that prevents tight packing and introduces mesoporosity.

3.6 SEM (Scanning Electron Microscope)

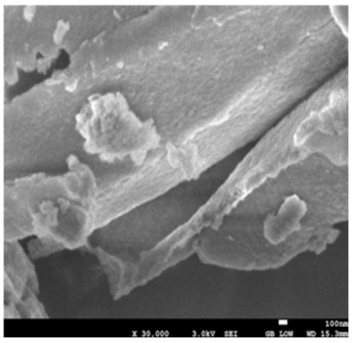

(a)

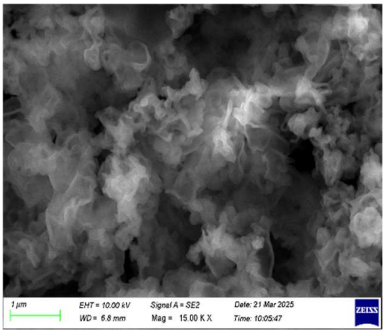

(b)

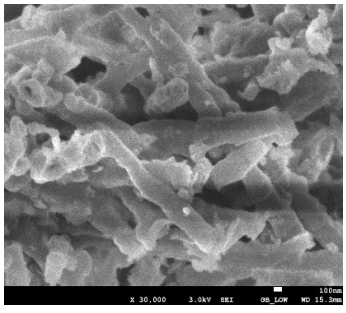

(c)

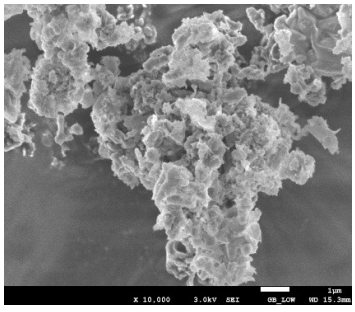

(d)

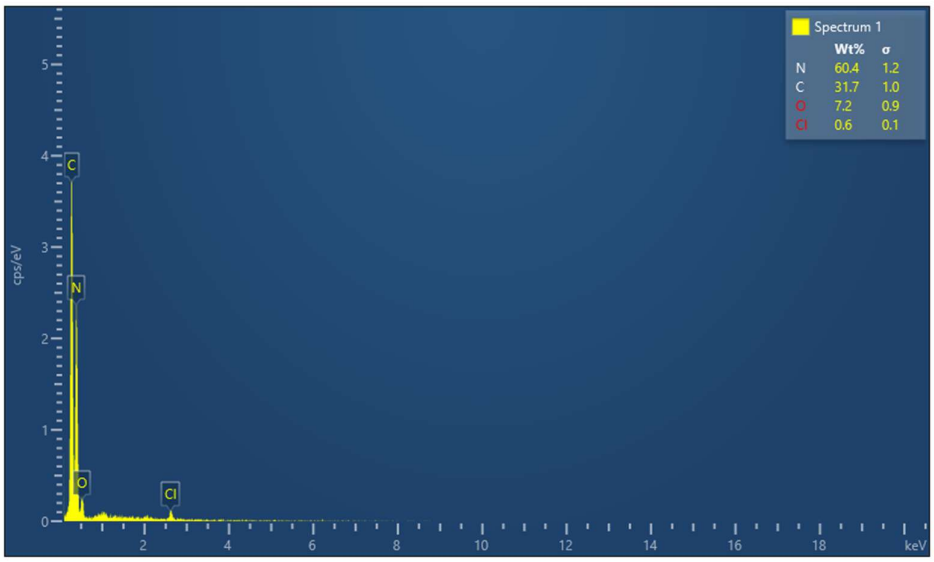

(e)

Figure 3.6 SEM images of (a) PCN (b) PTI (c) and (d) 5(0.5B-PTI)-PCN (e) EDX Analysis of 5(0.5B-PTI)-PCN

Scanning Electron Microscopy (SEM) was used to observe the surface structures of PCN, PTI and 5(0.5B-PTI)-PCN. The SEM image of PCN, image (a) shows thin, layered sheet-like structures. The smooth and flat surfaces suggest that the material has less surface roughness, which could limit how many active sites are available for photocatalytic reactions. The SEM image of PTI, image (b) shows a highly porous, layered nanosheet like-structure. This morphology is typical for PTI, which forms aggregated nanosheets or crumpled flakes due to their 2D nature. The image shows thin, overlapping sheet-like textures, suggesting high surface area – which is crucial for photocatalytic and adsorption applications.

The SEM image of 5(0.5B-PTI)-PCN, image (c) shows porous, thin and tube-like structure. This kind of porous framework is beneficial for increasing surface area and enhancing catalytic activity. The SEM image of 5(0.5B-PTI)-PCN, image (d) shows cloud-like agglomerates of crumpled nanosheets. These crumpled or folded layers increase surface roughness and provide more active sites for dye adsorption and catalytic reactions. The EDX (Energy-Dispersive X-ray Spectroscopy) provides information about the elemental composition of the surface analyzed. From image 3.6

(e), EDX analysis, nitrogen (N), carbon (C), oxygen (O) and Chlorine (Cl) show 60.4%, 31.7%, 7.2% and 0.6% respectively. Nitrogen is the major component of PTI and PCN framework (C-N bonding), carbon is the backbone element of polymeric carbon nitride, oxygen possibly from surface oxidation or adsorbed moisture and chlorine due to lithium chloride used in PTI synthesis.

3.7.1 RhB degradation

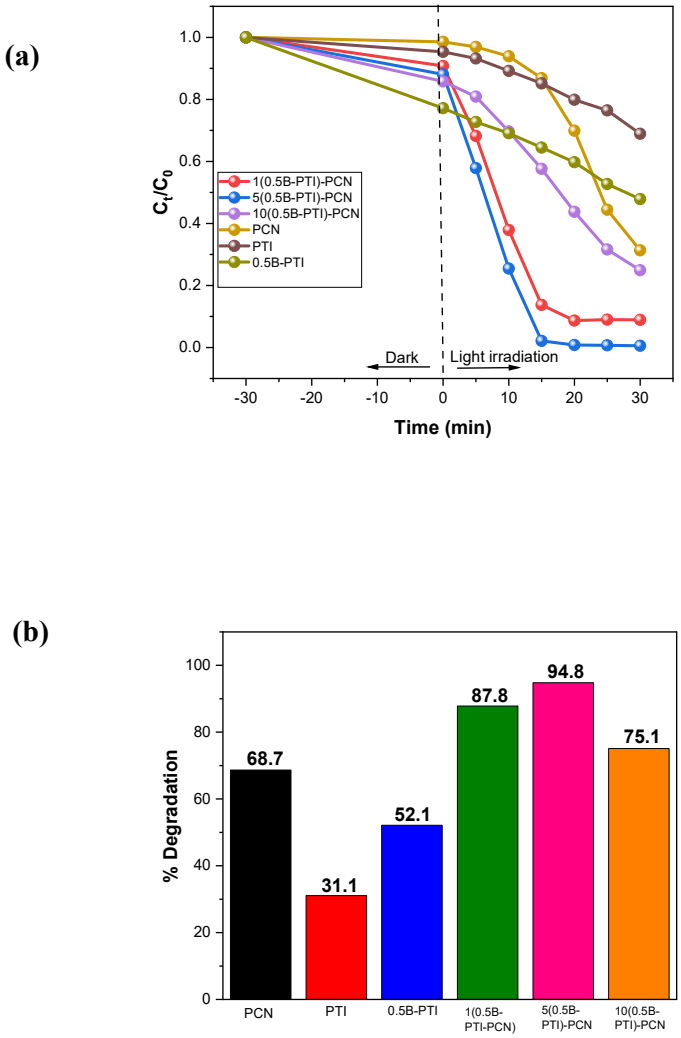

Figure 3.7 (a) Photocatalytic RhB (20 mg/L) degradation performance and (b) percentage degradation of RhB (20mg/L) at 30 minutes using various catalysts

The degradation of Rhodamine B (RhB) and reduction of Cr (VI) were investigated using a photocatalytic reactor equipped with 10 compact fluorescent lamps of 85 Watt. each and a magnetic stirrer. The radiation of fluorescent lamps is mostly visible light with a minimal proportion of UV (~ 3%).[5] Initially, 35 mg of the photocatalyst was dispersed in 100 mL RhB 20 mg/L solution, and the mixture was stirred in darkness for 30 minutes to establish adsorption-desorption equilibrium between the catalyst and RhB. Subsequently, the reaction mixture was exposed to light and aliquots were withdrawn at every 5 minute-interval to monitor the changes in RhB concentration. The absorbance of the samples was measured using a UV-Vis spectrophotometer (UV-1800 Shimadzu). After 30 minutes of light exposure, PCN and PTI achieved 68.7% and 31.1% degradation of RhB whereas the optimized heterostructure 5(0.5B-PTI)-PCN achieved enhanced 94.8% photocatalytic degradation. It may be due to high surface area and increase in visible light absorption of composite 5(0.5B-PTI)-PCN. Control experiment was conducted in the absence of light (dark) and photocatalyst (photolysis) confirmed the dependency of photoactivity on photon energy and the indispensable role of the photocatalyst in the degradation process.

3.7.2 Photocatalytic Cr (VI) reduction

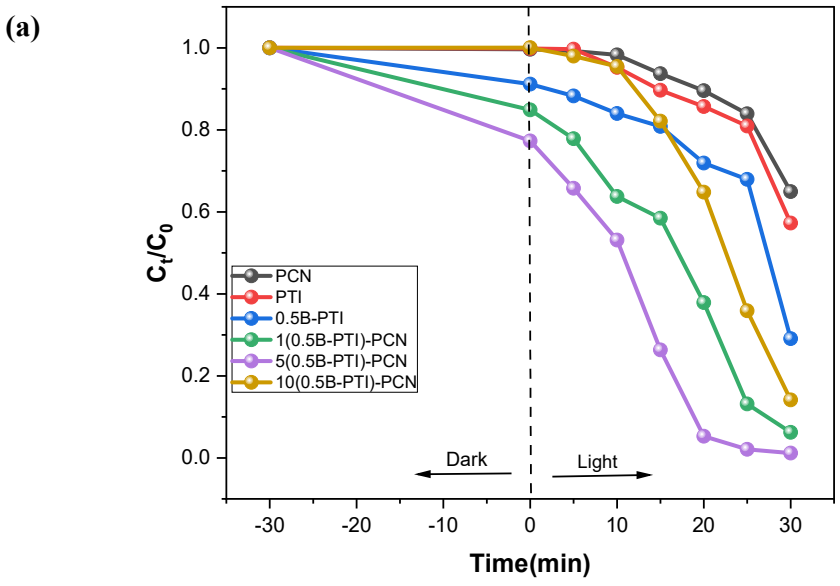

(b)

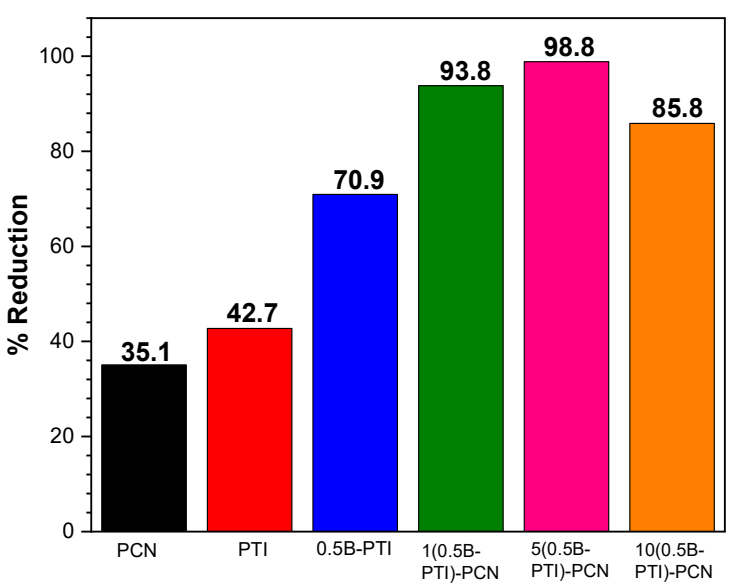

Figure 3.7.2 (a) Photocatalytic Cr (VI) reduction performance and (b) percentage reduction of Cr (VI) to Cr (III) at 30 min using various catalysts

The chromium (VI) reduction through photocatalysis was conducted using the setup described previously used. Initially, 50 mg of catalyst was dispersed in 50 mL Cr (VI) 20 mg/L solution and stirred in dark for 30 minutes to establish adsorption-desorption equilibrium. Subsequently, the suspension was irradiated with light, and sample aliquots were taken out after every 5 minutes to monitor changes in Cr (VI) concentration. UV-Vis spectrophotometer (UV-1800 Shimadzu) was employed to measure sample absorbance. After 30 minutes of light exposure, PCN and PTI achieved 35.1% and 42.7% reduction in chromium (VI) concentration, respectively. However, the heterostructure 5(0.5B-PTI)-PCN exhibited superior photocatalytic performance 98.8% reduction.

3.8 Effect of Quenchers on photocatalytic degradation of RhB degradation

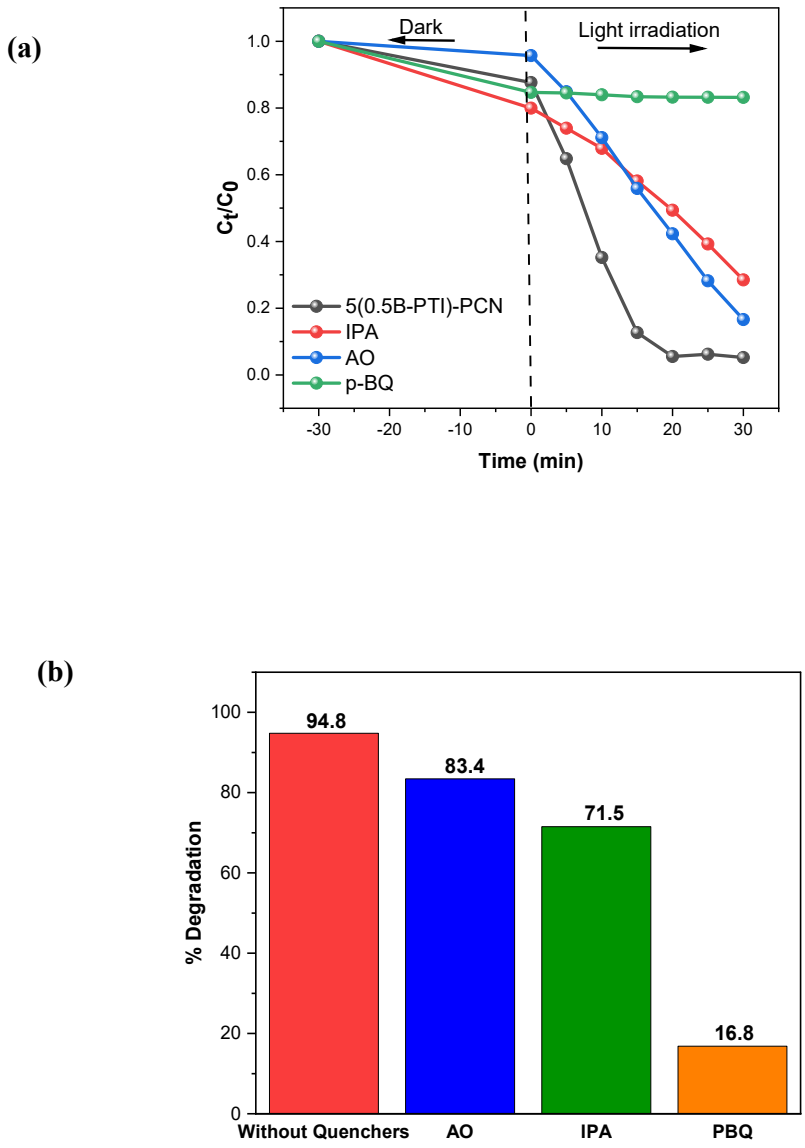

Figure 3.8 (a) Effect of quenchers on photocatalytic degradation of RhB (20 mg/L) and (b) Corresponding percentage degradation in presence of quenchers

To understand the photocatalytic degradation mechanism of RhB and identify the reactive oxidative species responsible for the degradation, scavenger experiments were conducted. Various scavengers such as isopropanol (IPA), ammonium oxalate (AO),

and para-benzoquinone (PBQ) (10^{-3}M) were utilized to trap hydroxyl radicals ($OH^{\bullet}$), holes (h^{+}), and superoxide radicals ($O^{2-\bullet}$) respectively. A decrease in photocatalytic activity in presence of IPA and AO suggests that $OH^{\bullet}$ and h^{+} have a minor role in RhB degradation. In contrast, the significant impact of PBQ on degradation efficiency indicates that $O^{2-\bullet}$ plays a major and crucial role in RhB degradation process.

From the degradation graph illustrated in figure 3.8 (b), the results demonstrate that among the reactive species tested, the $O^{2-\bullet}$ has a significant role in the degradation process, followed by $OH^{\bullet}$ while h^{+} has minimal effect under the given experimental conditions.

3.9 Photocatalytic degradation of RhB at different pH

(a)

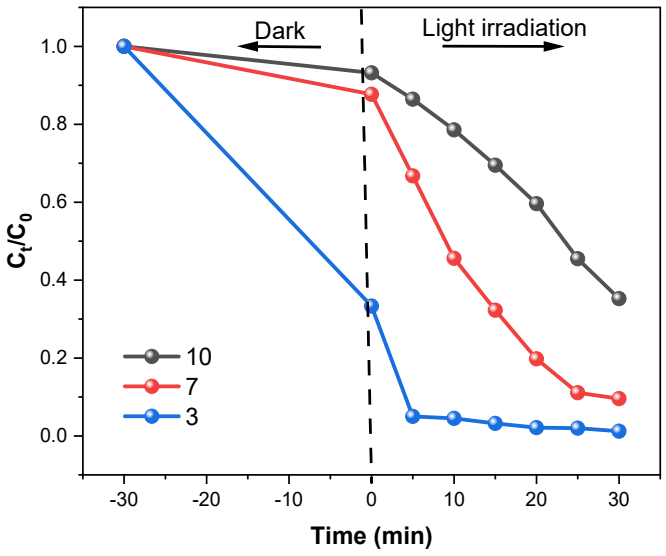

(b)

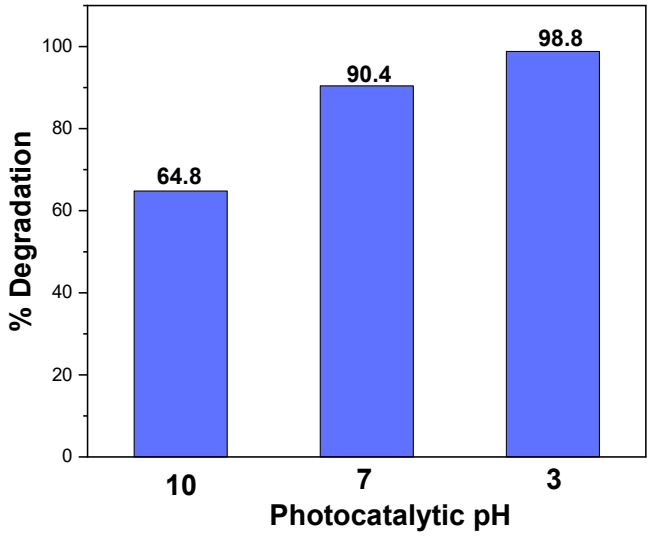

Figure 3.9 (a) Effect of pH on degradation of RhB (20mg/L) and (b) corresponding percentage degradation of RhB (20mg/L) at different pH

To determine the effect of pH on photocatalytic degradation of RhB, the experiments were conducted at different pH and degradation percentage is monitored in acidic, neutral and basic conditions. The pH of the RhB dye solution was adjusted using either hydrochloric acid (HCl) or sodium hydroxide (NaOH). The concentration of RhB was analysed for percentage degradation tendency at pH = 3, 7 and 10. The influence of pH on RhB degradation shows (Fig 3.9 a) that the catalyst achieves higher photocatalytic degradation efficiency at pH = 3, demonstrating 98.8% degradation tendency. As the pH rises, the degradation efficiency gradually decreases. Hence, at pH = 7 and pH=10, the percentage degradation efficiency was found to be 90.4% and 64.8%.

3.10 Recyclability Studies of 5(0.5B-PTI)-PCN heterostructure

Studies on the reusability of the composite concentrate on assessing its efficiency, sustainability and durability across multiple usage cycles. In this study, the recyclability of 5(0.5B-PTI)-PCN was carried out for degradation of RhB (20mg/L)

solution. The results indicated no prominent decrease in RhB degradation up to five cycles illustrating that the catalyst remains efficiently stable for up to four consecutive cycles.

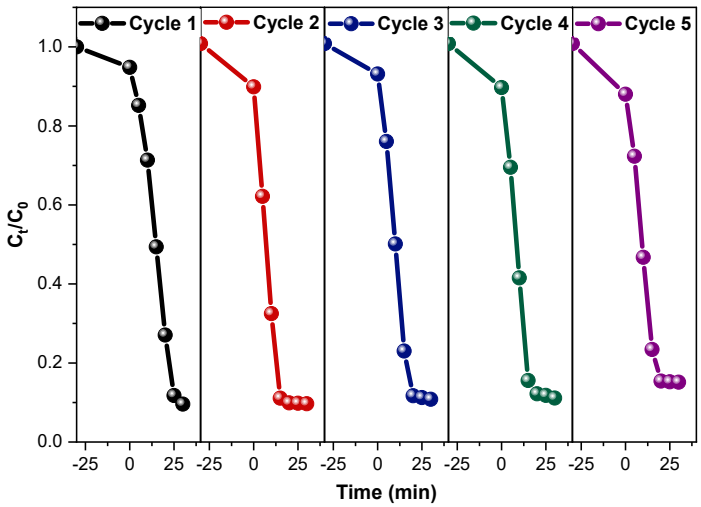

Figure 3.10 Recyclability studies of RhB degradation using 5(0.5B-PTI)-PCN heterostructure up to five cycles

References

1. Li, X., et al., *Preparation and characterization of graphitic carbon nitride through pyrolysis of melamine.* Applied Physics A, 2009. **94**: p. 387-392.
2. Ham, Y., et al., *Synthesis and photocatalytic activity of poly (triazine imide).* Chemistry–An Asian Journal, 2013. **8**(1): p. 218-224.
3. Ding, Z., et al., *Synthesis of transition metal-modified carbon nitride polymers for selective hydrocarbon oxidation.* ChemSusChem, 2011. **4**(2): p. 274-281.
4. Rawal, S.B., et al., *Design of visible-light photocatalysts by coupling of narrow bandgap semiconductors and TiO 2: effect of their relative energy band positions on the photocatalytic efficiency.* Catalysis Science & Technology, 2013. **3**(7): p. 1822-1830.
5. Natarajan, T.S., et al., *Study on UV-LED/TiO2 process for degradation of Rhodamine B dye.* Chemical Engineering Journal, 2011. **169**(1-3): p. 126-134.

CHAPTER 4

SUMMARY AND CONCLUSIONS

This chapter summarizes and concludes the enhanced photocatalytic performance of the binary heterostructure 5(0.5B-PTI)-PCN towards RhB dye degradation, Cr (VI) reduction and future prospects.

4.1 Summary and future aspects

Photocatalysis finds diverse applications in environmental and energy fields. The polymeric carbon nitride (PCN) photocatalyst has made tremendous progress in the remediation of harmful waste into environmentally sustainable products. However, PCN possesses some limitations and to overcome this limitation PCN is combined with PTI in the present work. The prepared binary heterostructure 5(0.5B-PTI)-PCN was successfully synthesized by calcination and solvent evaporation method. As a result, the properties of the synthesized heterostructure have significantly improved as compared to the individual components. In the binary heterostructure borophene acts as a mediator thereby allowing effective charge transfer between PTI and PCN. The 5(0.5B-PTI)-PCN exhibited much higher photocatalytic performance towards degradation of Rhodamine B dye and chromium (VI) reduction with a visible light irradiation of 30 minutes. The optimized heterostructure 5(0.5B-PTI)-PCN achieved 94.8% enhanced photocatalytic activity and 98.8% Cr (VI) reduction tendency. The increased photocatalytic activity of 5(0.5B-PTI)-PCN can be attributed to the high charge carrier mobility, decreased electron-hole recombination tendency, increase in the number of surface-active sites and enhanced visible light absorption tendency.

The future work plan of the study is to understand the detailed mechanism involved in Rhodamine B dye degradation and extend the usage of the photocatalyst in other applications such as H_2O_2 production.